An Optimized Method for Delivering Flow Tracer Particles to Intravital Fluid Environments in the Developing Zebrafish

Michael P. Craig,[1] Steven D. Gilday,[1] Dana Dabiri,[2] and Jay R. Hove[1]

Abstract

Growing evidence suggests that intravital flow–structure interactions are critical morphogens for normal embryonic development and disease progression, but fluid mechanical studies aimed at investigating these interactions have been limited in their ability to visualize and quantify fluid flow. In this study, we describe a protocol for injecting small ($\leq 1.0 \mu$m) tracer particles into fluid beds of the larval zebrafish to facilitate microscale fluid mechanical analyses. The microinjection apparatus and associated borosilicate pipette design, typically blunt-tipped with a 2–4 micron tip O.D., yielded highly linear ($r^2 = 0.99$) *in vitro* bolus ejection volumes. The physical characteristics of the tracer particles were optimized for efficient particle delivery. Seeding densities suitable for quantitative blood flow mapping (≥ 50 thousand tracers per fish) were routinely achieved and had no adverse effects on zebrafish physiology or long-term survivorship. The data and methods reported here will prove valuable for a broad range of *in vivo* imaging technologies [e.g., particle-tracking velocimetry, μ-Doppler, digital particle image velocimetry (DPIV), and 4-dimensional-DPIV] which rely on tracer particles to visualize and quantify fluid flow in the developing zebrafish.

Introduction

$\mathbf{F}$LOWING BIOFLUIDS have often been implicated as epigenetic regulators of morphogenic processes, but the complex relationships between flow and structure over the course of normal development remain largely unexplored. In addition to transporting heat, gases, biomolecules, and waste products throughout an organism, flowing fluids impose mechanical forces on their surrounding environments. These forces (e.g., shear, pressure, stretch) can be sensed at the cellular level[1,2] and often result in changes in gene and protein expression,[3] cell morphology,[4] and tissue organization.[5] Fluid forces are particularly important during development because the organism is undergoing rapid and often radical structural changes as it progresses toward its adult form. Prior studies have revealed that fluid flow plays a critical role in left-right patterning,[6–8] organogenesis,[9–11] kidney morphogenesis,[12,13] and cardiovascular development.[9,14] In addition, altered flow dynamics or disruptions to a particular fluid environment have been show to contribute to certain disease pathologies, including atherosclerosis,[15] lymphedema,[16] and polycystic kidney disease.[17,18]

The ability to visualize clearly and quantify fluid flow accurately within a living organism is a prerequisite for understanding the role of fluid forces in both development and disease. *In vivo* research into the role that flow plays in determining biological structure has been limited not only by technological constraints, but also by the inherent inaccessibility of internal fluid beds (e.g., blood, lymph, renal, cerebrospinal fluid). Commonly used mammalian and avian model organisms are optically opaque, and much of their early development takes place within the maternal reproductive system, making it very difficult to gain visual access without disturbing the normal physiologic environment. A number of noninvasive medical imaging modalities including magnetic resonance (MR),[19] computed tomography (CT),[20,21] and ultrasound,[22,23] have been adapted for use with small animals, but these technologies are not widely available, are prohibitively expensive, and frequently lack adequate spatial and/or temporal resolution for studying *in vivo* fluid dynamics at a scale consistent with a developing embryo. The emergence of the zebrafish as a canonical model of vertebrate biology, coupled with its genetic and phenotypic accessibility, rapid external development, and high degree of optical clarity throughout embryogenesis, make it ideal for studies involving *in vivo* flow imaging.[24]

Although the zebrafish has given scientists an unprecedented look into the intravital fluid milieu, the major challenge when studying microscale flows *in vivo* is obtaining a quantitative description of the flow field. Many techniques

[1]Department of Molecular and Cellular Physiology, University of Cincinnati College of Medicine, Cincinnati, Ohio.
[2]Department of Aeronautics and Astronautics, University of Washington College of Engineering, Seattle, Washington.

from engineering science have proven useful in this regard, the most straightforward and noninvasive of which involve recording and analyzing the movements of objects already circulating in high numbers in the fluid of interest. Erythrocyte mapping, for instance, has been used to describe the effects of vessel occlusion, adrenergic stimulation, and hypoxia on the global distribution of bloodflow in zebrafish.[25–27] The flow map generated base on the number of erythrocytes passing through sections of the vasculature is sufficient to compare differences in bulk flow, but the limited spatial resolution of the approach is too low for accurate measurement of wall shear stress or other hemodynamic parameters because of the large size of erythrocytes relative to the diameter of the containing blood vessels.

Endogenous tracers are not typically present in other fluid beds, so biofluid flow mapping generally requires injection of highly contrasting, neutrally buoyant tracers. At low to moderate seeding densities, the paths of injected tracer particles may be used to generate a vector map of the flow in an approach called particle tracking velocimetry (PTV). The PTV approach has been used to map blood flow velocity in the microcirculation,[28] aqueous flow in a rabbit model of argon laser iridotomy,[29] and pulsatile flow fields in a cerebrovascular side-wall aneurysm model[30] with sufficient resolution to estimate vorticity and wall shear stress. Further improvements in spatial resolution can be achieved using very high seeding densities in a technique called digital particle image velocimetry (DPIV). The DPIV approach does not rely on tracking the paths of individual tracers (as in PTV), but is instead implemented by matching speckle patterns in 'interrogation windows' (i.e., small subsets of the imaged area) between two consecutive microsecond-spaced images. DPIV better represents the complex features of the fluid flow by producing instantaneous, two-dimensional velocity vector plots. This type of quantitative flow map is extremely useful for calculating fluid dynamic parameters such as vorticity, as well as for deriving shear stresses on surrounding tissue, but such techniques have only recently been adapted for *in vivo* use at the microscale.[31] DPIV studies are only feasible if the experimenter is able to seed the fluid of interest with a relatively high density of tracer particles that mimic the complex details of the flow field. Thus, choosing appropriately sized particles with the correct physical and optical characteristics is critical to ensuring that measurements made using DPIV are accurate and reproducible. Furthermore, the tracers must be delivered to the fluid without seriously harming the animal, disrupting normal physiologic function, or altering the geometry or flow conditions within the flow field itself.

Microsphere-based *in vivo* applications such as the use of magnetic microspheres for targeted *in vivo* drug delivery,[29] DNA encapsulation,[28] and biofluid characterization (e.g., measurement of local blood viscosity,[32] flow patterns,[31] and oxygen saturation[33]) are gaining in popularity. Small fluorescent microspheres (0.02–0.04 micron diameter) have been used to perform zebrafish angiographies,[34] while much larger ones have been used to make two-dimensional strain measurements in the chick heart[35] and to measure regional blood flow in adult rainbow trout,[36] pigs, rabbits, and rats.[37] More recently, microspheres injected into the embryonic zebrafish bloodstream which had lodged into the heart wall were used to map endocardial motions using three-dimensional digital defocusing particle image velocimetry (3D-DPIV).[31] The increased use of microspheres in a variety of flow-mapping applications highlights the importance of developing a supporting infrastructure of detailed and efficient injection methodologies.

This study describes a method for efficient delivery of flow tracer particles into fluid beds within the developing zebrafish. The methodology was optimized for the zebrafish vasculature, but the same approach has also been implemented in the lymphatic and renal systems with only minor fluid bed-dependent modifications. Effective use of this method requires thorough consideration of numerous experimental parameters, including: 1) the fish's orientation when mounted in agarose and the choice of injection location; 2) the size, composition, surface properties, optical characteristics, and reactivity/toxicity of the tracer particles; 3) the material properties and internal tip diameter of the microneedle; 4) the applied injection pressure and the duration of this applied pressure; and 5) the number of injected boluses required to achieve the desired seeding density. This work addresses the importance of each of these parameters and highlights common problems and pitfalls one may encounter during experiments. Lastly, this study investigates the effects of injected flow tracer particles on normal zebrafish physiology and long-term survivorship. The detailed information reported here should prove valuable to researchers who are using DPIV, PTV or other *in vivo* imaging technologies that rely on tracer particles to visualize and quantify fluid flow in the developing zebrafish.

Materials and Methods

Zebrafish

Adult zebrafish were bred and maintained according to standard husbandry protocols[38,39] within the shared University of Cincinnati and Cincinnati Children's Hospital zebrafish facility. Adult fish were fed a mixed diet of Aquatox flake food (Aquatic Ecosystems, Inc.) and live *Artemia.* Temperature (26.5°–28.5°C), pH (7.1–7.4), conductivity (490–530 μS), dissolved oxygen (5.0–7.5 mg/L), and light cycle (14 h light/10 h dark) were electronically controlled and remotely monitored. Eggs were harvested and incubated in sterile system water at 28.5°C. Due to an abundance of available embryos and larva, WIK-strain zebrafish were used to practice, optimize, and test our flow tracer delivery methods. Once an optimal method had been established, *casper* (graciously provided by Leonard I. Zon, Children's Hospital Boston) pigment mutants were used for experiments requiring high quality intravital images. All animal protocols were reviewed and approved by the University of Cincinnati and Cincinnati Children's Hospital IACUC committees.

Agarose mounting

Zebrafish (2–7 days post fertilization) were embedded in 1.2% ultra-low melting point agarose containing 125 mg/L MS-222 (ethyl 3-aminobenzoate methanesulfonate salt, Sigma-Aldrich Co., Saint Louis, MO) for imaging by confocal microscopy. Fish were oriented on their side in a glass-bottom 35 mm petri dish.

Flow tracer particles

Multiple types and sizes of Fluosphere tracer particles (Molecular Probes, Eugene, OR) were evaluated in this study

because these tracers have high dye content throughout the plastic sphere, making them more resistant to photobleaching than those with an external fluorophore coating. For initial experiments, black 0.4 μm surfactant-free, carboxylate-modified (CML) latex particles were used. Subsequent optimization experiments utilized Fluosphere tracers of varying sizes (0.02–1.0 μm diameter) and with differing emission spectra [yellow-green (505/515 nm), red (580/605 nm), or dark red (660/680 nm)]. Prior to use, a 0.2% particle suspension was created by diluting the stock solution 1:10 in distilled water. One micron particles were further diluted to 1:100 in distilled water because lower use concentrations of the large particles were needed to prevent pipet tip clogging. All particle suspensions were sonicated for 5–10 minutes before use in order to prevent particle aggregation.

Glass microneedles

Microneedles were fabricated in-house using a laser-based horizontal micropipette puller (P-2000, Sutter Instruments, Novato, CA) and borosilicate capillary glass (1.0 mm OD, 0.75 mm ID, 10 cm length, World Precision Instruments, Sarasota, FL). Microneedles with an internal tip diameter of 2–4 μm and a straight, short taper were prepared using a single-line program with heat 340, filament 4, velocity 32, and delay 200. Any microneedle which did not meet specifications or appeared defective was discarded to ensure injection consistency.

Microneedle beveling, when utilized, was performed using a BV-10 microelectrode beveler (Sutter Instrument Company) fitted with an 104D fine grit abrasive wheel and an electrode impedence meter. Bevel progression was monitoring by back-filling microneedles with a 2 M salt solution and monitoring tip resistance. Beveling for 30 seconds was generally sufficient. Tip quality was confirmed by light microscopy.

Microinjection equipment and setup

Once anesthetized and mounted in agarose, zebrafish were place on an inverted microscope and positioned for optimal injection under low (10×) magnification. Microinjection was performed on a continuous zoom upright, wide-field confocal microscope (model MZ16FA, Leica Microsystems, Wetzlar, Germany) so that the injection target could be directly visualized during injection. The Leica microscope was fitted with a MA-TS heated stage (model MATS-TypeA, Leica Microsystems) to maintain consistency in zebrafish physiology. A glass microneedle was backfilled with a prepared suspension of flow tracer particles and loaded into a pneumatic microinjector (PLI-100, Harvard Apparatus, Holliston, MA). A 3-axis micromanipulator with sub-micron resolution (MP-85, Sutter Instruments) was used for microneedle tip positioning. The injection target site was chosen based on the fluid bed being targeted for seeding and the age of the animals being used. Small boluses of tracer particle suspension were injected into the biofluid of interest until the desired seeding density was achieved. Successful injections were verified by examining the flow field under higher magnification and noting the presence of circulating tracer particles. To be considered a success, a given injection attempt had to meet the following three criteria: 1) the glass microneedle was inserted into the appropriate anatomical location without breaking and without disfiguring the body wall, 2) the desired payload of flow tracer particles was

delivered to the fluid of interest without clogging the microneedle and without seriously damaging surrounding tissues, and 3) the zebrafish exhibited no adverse physiological changes immediately following the injection procedure.

Microinjections were also made using an inverted microscope (Zeiss Axiovert 200, Zeiss Microimaging Inc., Oberkochen, Germany) with a heated stage insert and matching micromanipulator. This approach proved useful particularly with injections into bloodstream confluence over the yolk sac because rapid high-speed confocal imaging could be accomplished without transferring mounted fish between microscopes. Injections performed on the inverted platform were generally well accommodated, particularly in 2–3 days post fertilization (dpf) *casper* embryos and in all fluid beds, although injections made on the inverted platform became progressively more challenging in older fish because tip placement and injection occurred on the side of the fish opposite to the one being viewed.

Microinjection volume calibration

The volume of each injected bolus is a function of the internal diameter of the microneedle tip, the injection pressure, and the duration of the applied pressure. To determine the volume of a single bolus for a range of microneedle tip diameters (2–4 μm) and injection pressures (3–20 psi), multiple boluses of 0.5 μm tracer particles suspended in distilled water were injected into light mineral oil using a 50 ms injection pulse. Each injected bolus formed an immiscible liquid sphere within the oil medium. The volume of each sphere was calculated based on its radius as measured using ImageJ (shareware, National Institutes of Health).

Long-term survivorship study

Two cohorts of 4 dpf WIK zebrafish were injected with either 0.2 or 1.0 μm red fluorescent carboxylate-modified microspheres or 1.0 μm red and monitored for physiological impairment and long-term survivorship over the course of 7 months. Multiple boluses (3.6 nL max volume, 10 sec between each bolus) were delivered into the bloodstream via the caudal vein until the vasculature was densely seeded with circulating particles. After successful injections were verified, the fish were removed from their agarose mounts and placed in sterile system water for 15–30 min, at which point they were observed under a dissecting microscope. Fish appearing healthy and physiologically normal were kept for the long-term study; fish showing signs of trauma or altered physiologic function as a result of the injection procedure were excluded. Each cohort of injected fish was raised in a separate tank in the zebrafish core facility to facilitate daily visual monitoring. Deaths, behavioral abnormalities, and morphological defects were recorded. After 7 months, the remaining injected fish were euthanized, weighed on a digital balance, and measured from nose to tail. Results were compared with un-injected controls.

Microscopy and imaging

In vivo tracer imaging was performed on a Zeiss Axiovert 200 inverted microscope equipped with an UltraView RS-3 live cell confocal scanner (PerkinElmer, Waltham, MA). Videos were collected using an EM-CCD camera (model

C9100-02, Hamamatsu Photonics K. K., Hamamatsu City, Shizuoka Prefecture, Japan). This system provided imaging capacity of 30 full frames per second at $1,000 \times 1,000$ pixels with a $>60\%$ quantum efficiency. Videos were analyzed using PIV software (PixelFlow, IO Industries, London, Ontario).

Results

Tip design

Borosilicate glass microneedles provided the best combination of strength and flexibility required during tip placement and insertion through the zebrafish body wall (Fig. 1). Aluminosilicate needles pulled with short tapers and matching tip diameters were too flexible to penetrate the body wall making access to all but the most superficial structures (e.g., the heart or the tail fin vasculature) unfeasible. Quartz needles, by contrast, proved too inflexible for general use and frequently broke during tip placement. For this reason, all subsequent injections were made using borosilicate needles.

We used microneedles with beveled tips to inject into the bloodstream of 7 dpf embryos in order to determine if the beveled tip design would improve penetration through the body wall without significant clogging. Tips with 30° or 45° bevels provided a very slight improvement in penetrance (as evidenced by a reduction in the magnitude of inward wall motion prior to puncture). These tips, however, were more difficult to calibrate, leaked during tip placement, and plugged far more often than blunt tips with similar tip sizes. Accordingly, the use of beveled tips was abandoned for routine injections.

Optimization of injection parameters

Injection volumes were calibrated by injecting half micron diameter microspheres into light mineral oil and measuring
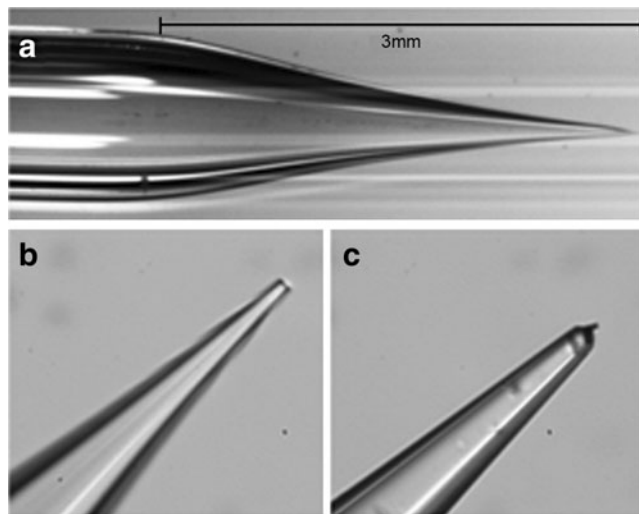

FIG. 1. Microneedle design. (a) Typical $5\,\mu$m tip [interior diameter (I.D.)] injection micropipette prepared using the laser-based horizontal puller. Higher magnification view of a blunt-tipped micropipette (b) shown as pulled, and a 30 degree beveled tip (c) prepared by backfilling the microneedle with a 2 M salt solution and monitor tip resistance while during fine grit abrasive grinding. (Tip beveling typically requires 30 seconds and is associated with a 15%–25% drop in tip resistance.)

the resulting water droplet diameter. The injection setup utilized herein provided a highly reproducible *in vitro* delivery of tracer particles. Half micron tracer bolus volumes correlated highly (Fig. 2, $R^2 = 0.999$) with the supplied injection pressures over the range of 0.6–2.5 nL (using a pulse pressure ranging from 2–20 psi). Further, bolus volumes correlated with tip diameter over the range of microneedle tip sizes most commonly used in this study (2.7–3.5 μm) (Fig. 3), allowing for a robust prediction of the number of microspheres injected per bolus (Table I). This range of tip sizes was large enough to minimize plugging while small enough to minimize tissue damage or leakage at the injection site. Changes in injection pressure had the greatest effect on bolus volume for the larger tip sizes (as expected), indicating that improved control over injection volume may be achieved by using higher source pressures. It should be noted that the larger (1.0 μm) tracers plugged 2–3 μm tips regularly such that low-volume and low-pressure boluses were generally not achievable, while high-pressure injections (10–20 psi) were erratic. The largest microneedles that could be used without tissue damage (i.e., those with 4–5 μm tip diameters) reduced clogging and improved bolus volume reproducibility somewhat, but controlled volume delivery could not be routinely achieved.

Volume control *in vitro* was very precise, while *in vivo* injection volumes exhibited increased variability due to tip clogging during body wall penetration. When performed by a trained technician, the microinjection protocol described in this study yielded successful injections approximately 75% of the time compared to a <30% success rate during initial attempts. Tip clogging was more problematic with deep tissue injections such as the kidney (pronephric duct) or lymphatic bed (thoracic duct), and the corresponding success rates for these locations were low (7%). Further, injections were generally more difficult as the fish aged, regardless of injection site. Through trial and error, optimal injection sites were chosen for agarose-mounted zebrafish at each age and for each fluid bed (Fig. 4). Seeding of the bloodstream was most easily accomplished via the convergent flow over the yolk sac between 20 and 48 hpf and via the common cardinal vein (CCV) between 48 and 96 hpf. From 4–7 dpf, the CCV was accessed by placing the pipet against the body wall just anterior to the caudal fin and cleithrum and gently moving the tip towards the tail to push the cleithrum out of the way. Injections performed later in juvenile and adult development were most easily made into the extreme caudal tail vasculature (either the caudal artery or vein).

Seeding of the pronephric duct, although challenging due to a small luminal diameter, was performed by injecting multiple, small boluses of tracers into the cloaca (i.e., against the flow) or into the trunk just anterior to the cloaca and dorsal to the aortic outflow. (The pronephric duct follows the dorsal aorta in the trunk. As a result, more than 50% of injections into the pronephric duct end up seeding the bloodstream.)

Injection into the primary lymphatic vessels via the thoracic duct can be performed by targeting the tissue space between the dorsal aorta and cardinal vein. Injections performed after the thoracic duct has completely formed (i.e., around 5 dpf) are possible, and tracers injected into lymph suggest a highly regurgitant flow pattern (data not shown). Tip clogging is common because injections occur into the thick trunk tissue and relatively late in development compared to other biofluid beds.

FIG. 2. *In vitro* injection volume calibration. Average single bolus volumes delivered at a range of supply pressures from an injection needle typical of those used for cardiovascular bed injections (3.1 micron tip I.D.). A 3 psi injection pressure was used in subsequent optimizations because the volume delivery was most reproducible at low psi. (Error bars ±1 standard deviation.)
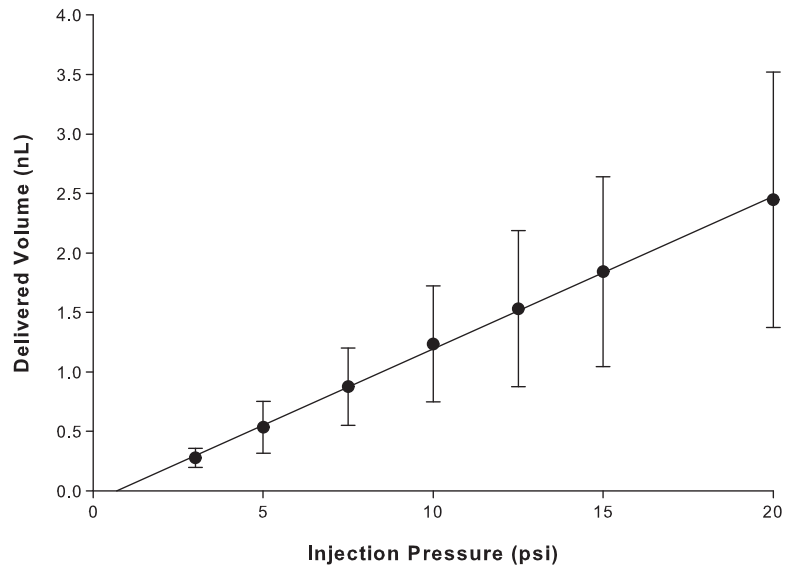
Tracer selection

Flow mapping experiments generally utilize the smallest resolvable tracers because small neutrally-buoyant tracers more accurately follow the local flow field. Six different sizes of flow tracers (0.02, 0.1, 0.2, 0.4, 0.5, and 1.0 μm) were tested to determine the minimum resolvable particle size (Table 2). The smallest particles (0.02 μm) were the easiest to inject and were quickly and uniformly distributed throughout the circulation. However, these flowing particles were too small to be individually resolved on our current imaging system, making them inappropriate for use in our PTV or PIV experiments but ideally suited for microangiographic mapping of the zebrafish vasculature, as described elsewhere.[16] Larger microspheres (0.4–1.0 μm) were more easily visualized as discrete entities as they flowed through the vasculature, thus making them desirable for flow mapping applications, but consistent delivery was challenging due to an increased incidence of clogged microneedles and tissue damage at the injection site. Further, maintaining a sufficient seeding density for PIV analysis was also difficult because a high percentage of the microspheres became permanently lodged in the vessel walls shortly after injection. (Approximately 20% of the dorsal aorta luminal wall is coated with 1.0 μm tracers at 30 min after injection.) Although these larger flow tracers may be suitable for some PTV experiments, the ideal tracers for PIV applications in the larval zebrafish are those with diameters ranging from 0.2–0.4 μm. Unlike their larger counterparts, particles in this size range were consistently injected near to the target seeding density (75,000 tracers per fish delivered in 2 boluses of 37,500) with no observable effects on circulation, surrounding tissue, or animal survivorship. Furthermore, >80% of the injected particles in this size range remained in circulation beyond 30 min after injection, allowing for extended imaging times.

FIG. 3. Volume injected (nL) based on tip diameter. The average single bolus volume delivered at a range of supply pressures (3–20 psi) for tips ranging in size from 2.7 to 3.5 microns is shown.
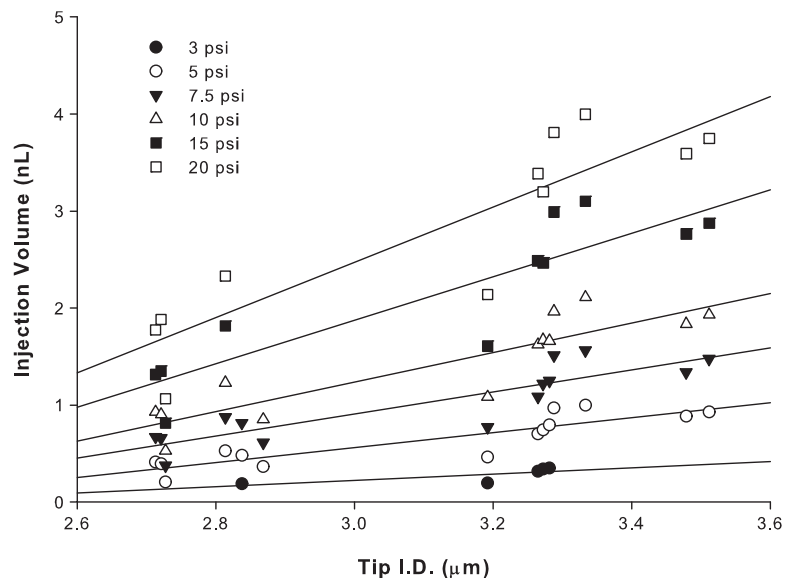
psi	Volume (nL)	Beads per bolus (x1000)
3	0.2 ± 0.1	8.5
5	0.5 ± 0.2	16
7.5	0.9 ± 0.3	27
10	1.2 ± 0.5	38
12.5	1.5 ± 0.7	47
15	1.8 ± 0.8	56
20	2.5 ± 1.1	75

Tracer density

Tracer density (ρ_p) must be close to the density of the surrounding fluid (ρ_f) so that paths of the 'neutrally buoyant' tracers accurately represent the complex motions of the biofluid they are suspended in. If $\rho_p > \rho_f$, the particles will rapidly settle out of the flow, whereas if $\rho_p < \rho_f$ the particles will "float", neither of which is desirable. Both situations result in additional drag and a resulting underestimation of local blood velocity. Most biofluids, including blood, have densities ranging from 1050–1064 kg m^{-3}.[40] For optimal density matching, we chose to use biologically inert polystyrene FluoSpheres with a density of 1050 kg m^{-3}. These tracer particles generally matched the velocity of nearby red blood cells in large vessels (e.g., the doral aorta) where RBCs flowed freely with only minimal physical interactions with adjacent cells or vessel walls, suggesting they *functionally* approxi-
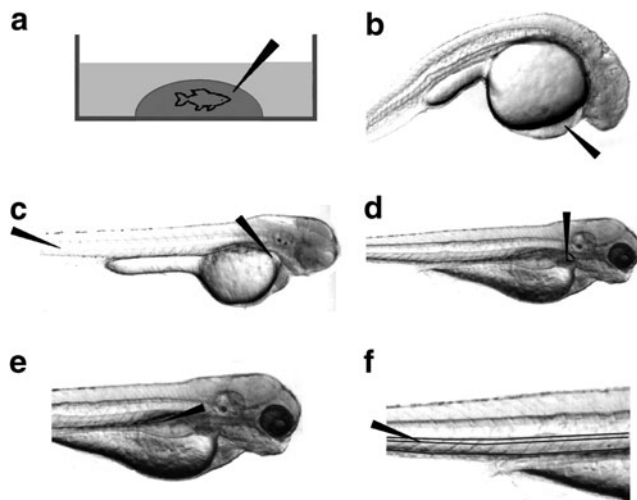

FIG. 4. Injection setup and targeting. Zebrafish are mounted in a drop of 0.6%–1.2% low-melting temperature agarose **(a)** containing anesthetic and covered with fish water (also containing anesthesia). Blood flow mapping in 24 hpf embryos is best performed by injecting into the confluence over the yolk sac **(b, arrow)**, 48 hpf into the common cardinal vein (CCV) or tail vein **(c, arrows)**, or into the CCV accessed by working the injection needle behind the cleithrum **(d)**. The pronephric ducts are best seeded on the anterior end near the pectoral fins **(e)**. Finally, seeding the lymphatics is best performed by injecting directly into the thoracic duct located between the dorsal aorta and the posterior cardinal vein **(f, top and bottom lines, respectively)**.

mated neutral buoyancy. Further, circulating tracers following complex flow patterns could be clearly discerned as they circulated throughout the vasculature.

Both fluorescent and nonfluorescent tracer particles were used in flow-mapping experiments. We successfully utilized 0.4 μm black latex beads at 1,250 fps for near-micron resolution flow mapping of the 3 dpf dorsal aorta in brightfield (Fig. 5), but image contrast was insufficient for automated tracer identification. Fluorescent microspheres provided much superior signal-to-noise and were used for all remaining experiments.

Seeding density

Seeding density requirements for various *in vitro* flow mapping algorithms have been previously established and are calculated from the imaged area, luminal diameter, particle size, and flow rate. While a detailed analysis of seeding density requirements for each fluid bed and imaging target is beyond the scope of this article, it is nonetheless useful to consider the following example:

2 dpf zebrafish total blood volume: 60 nl (estimated)**
Injection: ∼160,000 microspheres (10 boluses, 3.1 μm tip, 3 psi)
Imaging: 63X/1.2 N.A. objective, 512×512 CCD pixel area (67 μm × 67 μm)
Area taken up by DA: 6.24 μm × 67 μm × 0.5 μm =
Volume in center plane (0.5 μm thick): 2.2 pl
Percentage of total blood volume in imaged area: 0.04%
Approximate number of microspheres imaged: 557
Number of DPIV interrogation windows per vessel: 32
Number of particles per DPIV interrogation window: **17**

**This estimation is based on the observed number of particles per image field obtained using the specified injection parameters. This estimation is within the limits established in a study by Kopp et al.[41] in which 50 μL of blood was removed from 2 day old fish and resulted in a 66% decrease in red blood cell concentration (suggesting a maximum blood volume of 89 μL).

As shown above, injection of 160,000 microspheres in a total volume of 5 nL (an increase of approximately 8% in blood volume) is sufficient for DPIV analysis using a 63× objective. If lower magnifications are used, then the pixels in each image correspond to larger physical spaces, and it follows that a lower seeding density (in tracers per microliter of blood) is required to meet the recommended image density for successful DPIV.

The PTV approach relies solely on the ability of the user to identify and track the paths of a statistically significant number of tracer particles. Sections of simple linear, nonbranching vessels require fewer tracers than branching, pulsatile or highly turbulent flows. Generally, a seeding density of 1 tracer for every 100 pixels (or 200 tracers in the example above) should be considered the lower limit for PTV.

Tracer deposition and clearance

Tracer particles tend to adhere to one another and to endothelial borders, irrespective of their surface properties. The rate of tracer deposition on the vessel walls correlated inversely with particle size, with the small 0.02 μm tracers

TABLE 2. TRACER SELECTION GUIDE

Particle type	Tracer diameter	Advantages	Disadvantages	Potential in vivo applications
FluoSpheres	0.02 μm	Ease of injection, remain in circulation for many hours	Too small to be individually resolved	Microangiography
	0.1 μm	Ease of injection, remain in circulation for longer than 1 h	Not enough contrast to be resolved at high frame rates	PIV of slow velocity flows
	0.2 μm	Ease of injection, remain in circulation longer than 1 h, easy to visualize	Not enough contrast to be resolved at high frame rates	PIV of slow and medium velocity flows
Black CML latex	0.4 μm	Cheaper than fluorescent microspheres	Poor contrast with surrounding tissues	PIV of slow velocity flows
FluoSpheres	0.5 μm	High contrast with surrounding tissues, easy to visualize	Difficult to inject consistently, quickly lodge in vessel walls	PTV, PIV of slow and medium velocity flows
	1.0 μm	Very high contrast with surrounding tissues, easy to visualize even in fast flows	Difficult to inject consistently, quickly lodge in vessel walls, difficult to achieve required seeding densities	PTV, PIV of high velocity and/or turbulent flows
Native erythrocytes	~5–7 μm	Already present in the cardiovascular circulation, easy to visualize	Not present in all intravital fluids, do not capture microscale feature of the fluid flow	PTV

remaining in suspension the longest (over 24 h), and the large 1.0 μm remaining in circulation for less than 1 h. The rate of tracer deposition can be minimized by using tracer particles with a high surface concentration of carboxylic acid residues (similar to the large 10 and 15 μm tracers Invitrogen markets for measuring regional blood flow). The resulting weak neg-ative surface charge makes the microspheres somewhat hy-drophilic, a property which helps to prevent nonspecific binding to vessel walls and red blood cells in order to maxi-mize the number of tracers retained in circulation.

All particle sizes tended to deposit primarily in the cardinal vein. Minor depositions in the heart and fine vasculature were
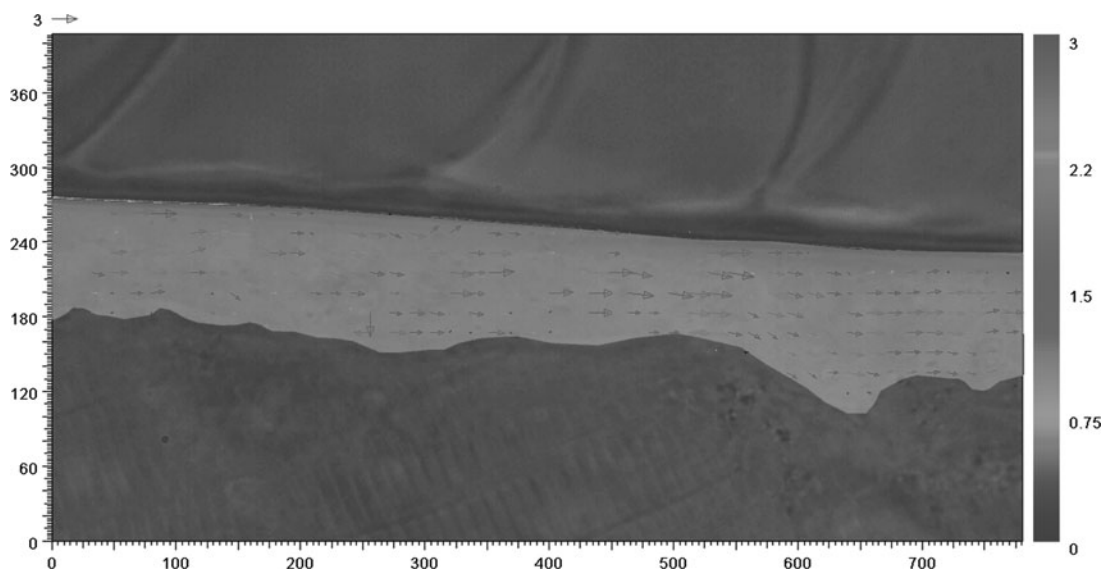

FIG. 5. DPIV-based blood flow mapping in the cardinal vein of a 77 hpf PTU-treated zebrafish using 0.3 μm black polystyrene, neutrally-buoyant microspheres. The vector map shown was generated in PixelFlow using a pair of images extracted from a 1250 fps video and this map was used as an overlay for the corresponding brightfield image to highlight vessel borders.
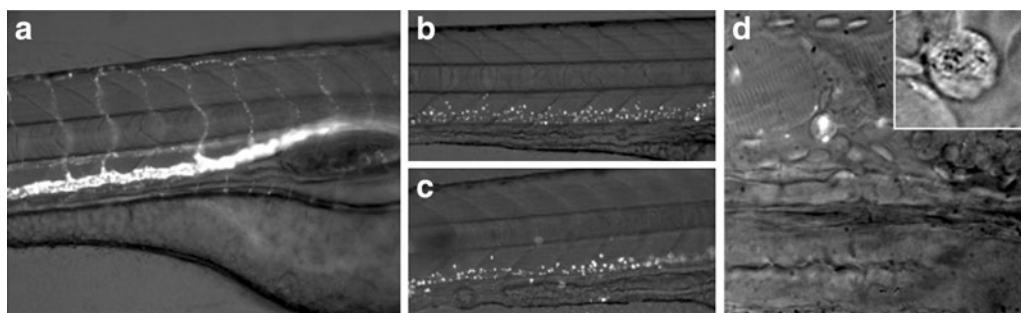
FIG. 6. Microsphere deposition and clearance. Circulating $0.4\,\mu$m tracers 24 hours post injection **(a)** and those deposited in the cardinal vein at 2 days **(b)** and 3 days **(c)** post-injection. By 3 days post-injection, tracer uptake was observed in noncirculating cells in the lumen of the cardinal vein (**d**, *insert at higher magnification*).

readily apparent in approximately 10% of injected fish. While it was impossible to quantify the number of clumped particles trapped in the vessel and heart walls microscopically, a qualitative comparison of particle distribution and overall fluorescence intensity over the first month showed no significant clearance of particles during that time. No particles were detected in zebrafish pronephric ducts, indicating that the tracers were not being cleared by glomerular filtration. Likewise, no tracers were detected in the digestive tracts of injected fish. No circulating cells internalized tracer particles, but a few cells lining the vessel walls did appear to accumulate a large amount of these particles (Fig. 6). A small number of fluorescent tracers were observed up to 1 month post injection.

Post-injection survivorship

High-seeding density microsphere injections ($\sim 350{,}000$–400,000 beads per fish) did not affect zebrafish survivorship and caused no obvious morphological changes in the animals. Zebrafish survivorship was similar to uninjected controls over the 30 week period of observation (Fig. 7, $n = 8$–10 per group). An initial drop in numbers occurred between 2–3 weeks of age when final swim bladder inflation occurs, *irrespective of treatment*. (This small drop in survivorship is typical in zebrafish husbandry because larvae are weaned onto a shrimp diet and because the swim bladder fails to inflate fully in a number of fish during this period. As a result, a number of juvenile animals rest on the tank bottom and die shortly after, unable to effectively scavenge for food. No abnormal swimming or feeding behaviors were noted in any of the control or injected fishes.)

Discussion

Basis of the methodology

Adaptation of macroscopic flow mapping technologies (such as 3-CCD DPIV) to the microscale has been accomplished in both brightfield[42] and fluorescent approaches.[43] The brightfield approach is inherently limited because the small particle sizes required for biofluid flow mapping in the zebrafish (e.g., submicron diameter particles) are inherently poorly contrasting. Further, the transparency of the embryonic and juvenile zebrafish which otherwise provides for excellent optical access to target tissues also makes it somewhat more difficult to distinguish fluid beds from neighboring

structures. We successfully utilized black latex beads for near-micron resolution flow mapping of the 3 dpf dorsal aorta in brightfield (see Fig. 5), but the signal-to-noise level in this approach was low enough that manual PTV was required.

Biolfuid flow mapping utilizing fluorescent microspheres imaged by standard confocal microscopy provides signal-to-noise levels sufficient for high-resolution and high-speed biofluid mapping. Fluorescent dyes are often encapsulated within the core of the microspheres (as opposed to being conjugated to the surface) in order to achieve high signal intensities with minimal photo-bleaching. Confocal fluorescent imaging provides greater signal-to-noise levels for even very small particles and is the method of choice for the vast majority of biological specimens. Despite the high fluorescent intensity of these microspheres, high camera frame rates and short exposures naturally lead to an overall diminished signal intensity and an associated decrease in signal-to-noise ratios. For high velocity or turbulent flows, such as those found in the beating heart, high frame rates are necessary in order to accurately correlate the motion of individual particles between frames. Increasing frame rates limit allowable exposure times, thus dimming the images and decreasing the contrast between the fluorescent tracers and the surrounding environment making it necessary to use high quantum-efficiency
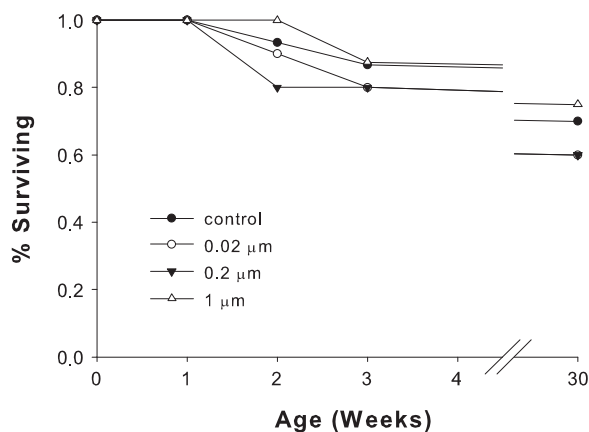

FIG. 7. Post-injection survivorship of embryos injected with a high seeding density of a range of microspheres sizes at 4 dpf. The initial number of injected embryos was set to 100% and all subsequent values are shown relative to that initial number.

single-line or back-thinned detectors. High speed florescent imaging at >750 fps using a raster-scanning single line CCD (e.g., Zeiss 5Live confocal) provides the imaging speed and spatial resolution to map highly dynamic flows using 2-color DPIV. Mapping of faster flows (e.g., adult heart flow) or highly turbulent flows (e.g., zebrafish pronephric flow surrounding motile renal cilia) are likely still beyond the temporal imaging capabilities of cutting-edge fluorescent confocal systems, so crude bulk-flow (e.g., dye-front) measurements will have to suffice in the short term.

Microsphere selection

Intravital flow mapping requires seeding the fluid bed of interest with high contrast tracer particles which accurately reflect fluid velocity (i.e., have 'neutral buoyancy'), do not clump, and remain suspended in the biofluid being imaged long enough to complete the desired experiment. While this generally dictates the use of a fluorescent confocal approach, we successfully mapped cardiovascular blood flow in the larval zebrafish cardinal vein using black-dyed polystyrene particles and associated high-speed brightfield imaging. With sufficient lighting, we utilized this approach at frame rates up to 1250 fps, sufficient for blood flow mapping in a 77 hpf zebrafish with pharmacologically blocked pigmentation (elicited with phenyl-thiourea) (Fig. 5). While this approach offers superior temporal resolution, it requires a modified light path and sophisticated post-processing software in order to make it a volumetric (3D) flow-mapping tool.[42] (Automated DPIV requires uniformity of background and high signal-to-noise levels not often afforded by brightfield approaches. A color-coded approach has been developed to circumvent this issue,[42] but high-speed color cameras are cost-prohibitive and not widely available in a biology lab setting.)

A more readily accessible approach is to use dye-embedded fluorescent microspheres which provide superior contrast and are amenable to tomographic (i.e., optical sectioning) microscopy, making them particularly useful in the zebrafish model. The high fluorescent output of these tracer particles makes them ideal for use in older embryos and larvae when tissue opacity and sample thickness begin obscure the target fluid bed. The FluoSpheres used in this study and for previous DPIV-based studies in the zebrafish[31] are intensely fluorescent and show no appreciable signal loss due to photobleaching. Fluorescent confocal videos taken using a 488 nm solid-state laser (100 mW, 4% power), a 100×/1.2 numerical aperture microscope objective, and a Zeiss 5 Live high-speed confocal scanner possessed sufficient signal-to-noise for automated particle tracking at 500 fps with no detectable photobleaching or damage to the imaged or surrounding tissue (data not shown). When performed in lowly-pigmented zebrafish mutant lines (e.g., *Blingless*[44,45] and *Casper*[46]), biofluid flow mapping may be performed well into the first several weeks of larval development.

Tracer particles with shorter emission wavelengths generally have higher quantum efficiencies but lower penetrance than those with longer emission wavelengths, thus requiring the researcher to match the chosen application to tracers with appropriate spectral characteristics. Green and blue emitting tracers accommodate the high frame rates required for mapping blood flow in the heart or vasculature or the highly turbulent renal flow around motile pronephric cilia. Red emitting tracers, by contrast, are better suited for deep or opaque tissue mapping, particularly in older fish, and are useful in later lymphatic vessel flow mapping. If it is possible to choose GFP or mCherry fluorescent reporter lines [e.g., TG(Fli:GFP) and TG(Flk1:mCherry)] with different emission profiles than the flow tracers being used, it becomes possible to image the vessel wall positions and flow profiles concurrently, thus providing a methodology for robust biofluid mapping. The green line (488 nm) is most frequently reserved for GFP-tagged structural imaging such as the vascular endothelial fluorescence in the fli:GFP zebrafish embryo. For that reason, we chose the near-red 0.4 micron microspheres for the bulk of our flow mapping studies. These tracers provide sufficient intensity for dual-channel imaging (i.e., GFP and red microsphere) at over 100 frames per second and much higher if a single-channel reduced-frame size approach is used, sufficient for virtually all biofluid flow mapping experiments.

In addition to the emission profiles of fluorescent and nonfluorescent tracers, the surface properties of the fluorescent microspheres can affect clumping and deposition on vessel walls. Carboxylated spheres are routinely used for blood flow mapping because they carry a slight negative charge that helps minimize both aggregation and deposition. These microspheres appear to work equally well for zebrafish blood, renal and lymphatic flows, with carboxylated tracers remaining suspended in the flow long enough for biofluid flow mapping.

Our study determined that particle size was the biggest factor in determining how long beads remained in circulation for effective flow mapping. As a general rule, larger luminal diameters accommodate larger tracer particles and faster flow rates tend to keep large tracers suspended longer. Tracer size should therefore be chosen based on target lumen size and flow rate for each application. This study has provided a rough guide for making this selection (Table 2). For instance, mapping of slow intraocular fluid flow (large measurement volume) would utilize larger (e.g., 2 μm) beads than fast, pulsatile peripheral vasculature flow (e.g., 0.2 μm beads).

Preparation of micropipettes and zebrafish for injection

The optimal injection pipet taper is somewhat dependent on the physical properties of the tracer particles and the depth of the injection target, but a sort taper (e.g., 30–45 degrees) is generally preferred. Needle-like pipets plug readily even when the tracer size is a fraction of the tip ID. Conversely, broader tips cause more peripheral tissue damage. Empirical testing is required to determine the proper balance between plugging and tissue damage for any given application. We routinely use borosilicate glass pipets. Other types of glass may work for individual fluid beds, but borosilicate glass provides the balance between strength and flexibility needed to penetrate the body wall and prevent breakage. The added strength of quartz glass or the added flexibility of alumina silicate glass make performing injections more difficult and the added expense for these alternatives is not merited. Beveled tips are generally not required, but may be of some utility in deep tissue injections using older fish. All tip sizes and contours clog to some degree, even when the microsphere diameter is several-fold less than the interior tip diameter. Backfilling the injection needle using a gel-loading tip rather than vacuum filling helps to minimize this clogging.

Mounting zebrafish in agarose makes it possible to adjust their orientation for the best optical access to the desired biofluid bed. Depending on the imaging target, injection and mounting may require different orientations. We routinely agarose-mounted and imaged fish on an inverted microscope such that pipet placement and injection occurred from above while the placement and injection was visualized from below the fish (through the body wall). This approach allowed *immediate* imaging without the need for remounting or further manipulation. Injections may also be performed using an upright microscope with long working-distance objectives that provide the working distance needed to accommodate the injection hardware. Alternatively, fish may be injected on a standard dissecting microscope and transferred to the fluorescent confocal for imaging, but that may require additional equipment and the transfer cuts into the sometimes narrow imaging window when tracers are circulating.

Imaging of heart blood flow, in particular, requires mounting the fish with the ventral side touching the bottom of the coverslip on our inverted system. There are no exposed targets for microinjection when fish are mounted in this manner, so we frequently injected fish on their side and then remounted for subsequent imaging. We have also experimented with standard embryo injection trays (as described in the Zebrafish Book[47]) as a means of avoiding remounting. These trays provide a solid backstop that improves tip penetration through the body wall, but heavy anesthetic is required for this approach because even moderately anesthetized fish twitch during body wall puncture.

Injection

The injection location should be chosen such that it is physically removed from the imaging target and any localized tissue damage from the injection itself will have minimal effect on the imaging target. Further, since deep tissue injections tend to plug more and cause more localized tissue damage, a peripherally located injection target should be chosen wherever possible. Blood flow mapping is most easily accomplished by injection into the confluence over the yolk sac at 1 dpf, into the heart at 2–3 dpf, and into the cardinal tail vein thereafter. The geography of the fluid bed may, however, dictate suboptimal injection locations or regimes. The discontinuous nature of the developing thoracic duct makes early lymphatic flow mapping difficult. Similarly, the linear nature of renal outflow requires seeding of the fluid bed near its origin at the glomerulus. The single zebrafish glomerulus is difficult to inject directly due to its location deep within the zebrafish trunk. For that reason, renal flow mapping is effectively limited to injections into the anterior pronephric duct or cloaca.

Calibrated volume delivery of bead suspensions using a $3\,\mu m$ tip ID was highly reproducible over the range of volumes typically required for small animal flow mapping (0.6–4 nL per bolus). Based on stroke volume measurements, we estimate that the total volume of blood in a 2 dpf zebrafish is between 50 and 90 nL, so a 5 nL injection would constitute an instantaneous 8% increase in blood volume. Our typical injection setup ($3\,\mu m$ I.D. tips, 5 psi injection pressure) delivered 5 nL of volume with no obvious physiological side-effects. Obtaining the desired tracer seeding density in the biofluid being imaged, therefore, is achieved by either maximizing the concentration of tracers in the injection needle or injecting multiple spaced boluses. Since it is desirable to keep the tracer density in the needle low to prevent clumping and to keep injected volumes low to minimize the effect(s) on zebrafish physiology, the optimal balance between these parameters must be determined empirically for any given application. Finally, we found no evidence that seeding blood flow at high levels had any observable effect on zebrafish physiology or long-term survivorship despite the fact that microspheres remained lodged in the walls of the cardinal vein for a month or more with no obvious clearance (e.g., glomerular filtration or gill passage).

Summarized methodology

Injection of $0.4\,\mu m$ fluorescent microspheres into the bloodstream of an agarose-mounted 48 hpf embryo is most easily performed using a short-tapered $3\,\mu m$ borosilicate injection pipet backfilled with a 0.2% suspension of microspheres targeted to the convergent flow over the yolk sac and delivered in 50 ms pulses to achieve a total injection volume of approximately 5 nL. Adapting this setup to other ages or fluid beds requires careful consideration of biofluid flow rates, luminal diameter(s), and tissue environment of the injection target.

Conclusion

The data presented herein are intended to serve as a guide for a broad range of researchers in bioengineering, fluid mechanics, and physiology laboratories. The findings reported here have direct applications to PTV, μ-Doppler, DPIV, and 4D-DPIV, which rely on tracer particles to visualize and quantify fluid flow in the developing zebrafish.

Acknowledgments

Disclosure Statement

No competing financial interests exist.

References

1. Lehoux S, Castier Y, Tedgui A. Molecular mechanisms of the vascular responses to haemodynamic forces. J Int Med 2006;259:381–392.
2. Chien S. Mechanotransduction and endothelial cell homeostasis: The wisdom of the cell. Am J Physiol Heart Circ Physiol 2007;292:H1209–1224.
3. Wasserman SM, Topper JN. Adaptation of the endothelium to fluid flow: *In vitro* analyses of gene expression and *in vivo* implications. Vasc Med 2004;9:35–45.
4. Helmlinger G, Geiger RV, Schreck S, Nerem RM. Effects of pulsatile flow on cultured vascular endothelial cell morphology. J Biomech Eng, 1991;113:123–131.

5. Eaton S, Julicher F. Cell flow and tissue polarity patterns. Curr Opinion Genet Devel 2011;21:747–752.

6. Okada Y, Takeda S, Tanaka Y, Izpisua Belmonte JC, Hirokawa N. Mechanism of nodal flow: a conserved symmetry breaking event in left-right axis determination. Cell 2005;121:633–644.

7. Cartwright JH, Piro O, Tuval I. Fluid-dynamical basis of the embryonic development of left-right asymmetry in vertebrates. Proc Natl Acad Sci USA 2004;101:7234–7239.

8. Bisgrove BW, Essner JJ, Yost HJ. Multiple pathways in the midline regulate concordant brain, heart and gut left-right asymmetry. Development 2000;127:3567–3579.

9. Sidi S, Rosa FM. [Mechanotransduction of hemodynamic forces regulates organogenesis]. Med Sci (Paris) 2004;20:557–561.

10. Hove JR, Koster RW, Forouhar AS, Acevedo-Bolton G, Fraser SE, Gharib M. Intracardiac fluid forces are an essential epigenetic factor for embryonic cardiogenesis. Nature 2003;421:172–177.

11. Chatzizisis YS, Coskun AU, Jonas M, Edelman ER, Feldman CL, Stone PH. Role of endothelial shear stress in the natural history of coronary atherosclerosis and vascular remodeling: Molecular, cellular, and vascular behavior. J Am Coll Cardiol 2007;49:2379–2393.

12. Nauli SM, Alenghat FJ, Luo Y, Williams E, Vassilev P, Li X, et al. Polycystins 1 and 2 mediate mechanosensation in the primary cilium of kidney cells. Nat Genet 2003;33:129–137.

13. Serluca FC, Drummond IA, Fishman MC. Endothelial signaling in kidney morphogenesis: A role for hemodynamic forces. Curr Biol 2002;12:492–497.

14. Fisher SA, Langille BL, Srivastava D. Apoptosis during cardiovascular development. Circ Res 2000;87:856–864.

15. Cunningham KS, Gotlieb AI. The role of shear stress in the pathogenesis of atherosclerosis. Lab Invest 2005;85:9–23.

16. Coffindaffer-Wilson M, Craig MP, Hove JR. Normal interstitial flow is critical for developmental lymphangiogenesis in the zebrafish. Lymphat Res Biol 2011;9:151–158.

17. Ong AC, Wheatley DN. Polycystic kidney disease– The ciliary connection. Lancet 2003;361:774–776.

18. Kramer-Zucker AG, Olale F, Haycraft CJ, Yoder BK, Schier AF, Drimmond IA. Cilia-driven fluid flow in the zebrafish pronephros, brain and Kupffer's vesicle is required for normal organogenesis. Development 2005;132:1907–1921.

19. Kabli S, He S, Spaink HP, Hurlstone A, Jagalska ES, De Groot HJ, Alia A. In vivo magnetic resonance imaging to detect malignant melanoma in adult zebrafish. Zebrafish 2010;7:143–148.

20. Ma R, Aturuttis A, Ntziachristos V, Razansky D. Multispectral optoacoustic tomography (MSOT) scanner for whole-body small animal imaging. Opt Express 2009;17:21414–21426.

21. Vasquez SX, Hansen MS, Bahadur AN, Hockin MF, Kindlmann GL, Nevell L, et al. Optimization of volumetric computed tomography for skeletal analysis of model genetic organisms. Anat Rec (Hoboken) 2008;291:475–487.

22. Ho YL, Shau YW, Tsai HJ, Lin LC, Huang PJ, Hsieh FJ. Assessment of zebrafish cardiac performance using Doppler echocardiography and power angiography. Ultrasound Med Biol 2002;28:1137–1143.

23. Turnbull DH, Bloomfield TS, Baldwin HS, Foster FS, Joyner AL. Ultrasound backscatter microscope analysis of early mouse embryonic brain development. Proc Natl Acad Sci USA 1995;92:2239–2243.

24. Hove JR. In vivo biofluid dynamic imaging in the developing zebrafish. Birth Defects Res C Embryo Today 2004;72:277–289.

25. Schwerte T, Pelster B. Digital motion analysis as a tool for analysing the shape and performance of the circulatory system in transparent animals. J Exp Biol 2000;203:1659–1669.

26. Schwerte T, Fritsche R. Understanding cardiovascular physiology in zebrafish and Xenopus larvae: The use of microtechniques. Comp Biochem Physiol A Mol Integr Physiol 2003;135:131–145.

27. Schwerte T, Uberbacher D, Pelster B. Non-invasive imaging of blood cell concentration and blood distribution in zebrafish Danio rerio incubated in hypoxic conditions in vivo. J Exp Biol 2003;206:1299–1307.

28. Ravnic DJ, Zhang YZ, Tsuda A, Pratt JP, Huss HT, Mentzer SJ. Multi-image particle tracking velocimetry of the microcirculation using fluorescent nanoparticles. Microvasc Res 2006;72:27–33.

29. Yamamoto Y, Uno T, Shisida K, Xue L, Shiraishi A, Zheng X, Ohashi Y. Demonstration of aqueous streaming through a laser iridotomy window against the corneal endothelium. Arch Ophthalmol 2006;124:387–393.

30. Liou TM, Liou SN, Chu KL. Intra-aneurysmal flow with helix and mesh stent placement across side-wall aneurysm pore of a straight parent vessel. J Biomechan Engineer 2004;126:36–43.

31. Lu J, Pereira F, Frazer SE, Gharib M. Three-dimensional real-time imaging of cardiac cell motions in living embryos. J Biomed Opt 2008;13:014006.

32. Haidekker MA, Theodorakis EA. Molecular rotors— Fluorescent biosensors for viscosity and flow. Org Biomol Chem 2007;5:1669–1678.

33. Liu KJ, Grinstaff MW, Jian J, Suslick KS, Swartz HM, Wang W. In vivo measurement of oxygen concentration using sonochemically synthesized microspheres. Biophys J 1994;67:896–901.

34. Kamei M, Isogai S, Weinstein BM. Imaging blood vessels in the zebrafish. Methods Cell Biol 2004;76:51–74.

35. Ling P, Taber LA, Humphrey JD. Approach to quantify the mechanical behavior of the intact embryonic chick heart. Ann Biomed Eng 2002;30:636–645.

36. Taylor S, Egginton S, Taylor E. Seasonal temperature acclimatisation of rainbow trout: Cardiovascular and morphometric influences on maximal sustainable exercise level. J Exp Biol 1996;199:835–845.

37. Bernard SL, Ewen JR, Barlow CH, Kelly JJ, McKinney S, Frazer DA, Glenny RW. High spatial resolution measurements of organ blood flow in small laboratory animals. Am J Physiol Heart Circ Physiol 2000;279:H2043–2052.

38. Coffindaffer-Wilson M, Craig MP, Hove JR. Normal interstitial flow is critical for developmental lymphangiogenesis in the zebrafish. Lymphat Res Biol 2011;9:151–158.

39. Westerfield M, The Zebrafish Book. A guide for the laboratory use of zebrafish (Danio rerio). 5th ed. 2007.

40. Baez R, Romero A, Soto G. Properties of biofluids in the human body. Blood Pressure 2004:1–35.

41. Kopp R, Pelster B, Schwerte T. How does blood cell concentration modulate cardiovascular parameters in developing zebrafish (Danio rerio)? Comp Biochem Physiol Mol Integ Physiol 2007;146:400–407.

42. Tien WH, Kartes P, Yamasaki T, Dabiri D. A color-coded backlighted defocusing digital particle image velocimetry system. Exp Fluids 2008;44:1015–1026.

43. Pereira F, Lu J, Castano-Graff E, Gharib M. Microscale 3D flow mapping with mu DDPIV. Exp Fluids 2007;42:589–599.

44. Karlsson J, von Hofsten J, Olsson PE. Generating transparent zebrafish: A refined method to improve detection of gene expression during embryonic development. Marine Biotechnol (New York, N.Y.) 2001;3:522–527.

45. White RM, Sessa A, Burke C, Bowman T, LeBlanc J, Ceol C, et al. Transparent adult zebrafish as a tool for *in vivo* transplantation analysis. Cell Stem Cell 2008;2:183–189.

46. Kent ML, Buchner C, Watral VG, Saanders JL, Ladu J, Peterson TS, Tanguay RL. Development and maintenance of a specific pathogen-free (SPF) zebrafish research facility for *Pseudoloma neurophilia*. Dis Aquatic Org 2011;95:73–79.

47. Westerfield M. *The Zebrafish Book: A Guide for the Laboratory Use of Zebrafish.* 4 ed. 2000, Eugene, OR: University of Oregon Press.

Address correspondence to:
Michael P. Craig, M.S.
Department of Molecular and Cellular Physiology
University of Cincinnati College of Medicine
231 Albert Sabin Way
Cincinnati, OH 45267-0576

E-mail: Craigm@mail.uc.edu